Article

Stored Photoelectrons in a Faradaic Junction for Decoupled Solar Hydrogen Production in the Dark

Qiushi Ruan[1,2,a]*, Xufeng Xi[1,a], Bingzhen Yan[a], Lingqiao Kong[a], Chaoran Jiang[b]*, Junwang Tang[c], ZhengMing Sun[a]*

SUMMARY

Considering the intermittent solar energy availability, storing excess photon energy for subsequent use in dark represents a decoupled solar energy utilization strategy, resembling dark reduction process in natural photosynthesis. Multielectron accumulation is key to such dark photosynthesis. However, accompanied by energy loss of stored photoelectrons, dark hydrogen generation suffers from low efficiency. Here, we demonstrate the efficient release of hydrogen from methanol-reforming in the dark over a TiO_x/CN faradaic junction. Under irradiation, photoelectrons generated from polymeric carbon nitride (CN) were stored in an electron pool at the TiO_x/CN interface with negligible energy loss via a quasi-isoenergetic process. Those stored photoelectrons slowly release active electrons for proton reduction, resulting in decoupled hydrogen generation in dark. This storing process describes accumulation and gradual release of photoelectrons in a faradaic junction, which enables the on-demand utilization of solar energy for hydrogen generation, thereby alleviating the mismatch between solar hydrogen demand and sunlight availability.

INTRODUCTION

Intermittent solar energy at spatial and temporal scales mismatches the energy demand of our daily activity and industrial production while storing excess solar energy in batteries or transmitting electricity across regions adds unsustainable financial and environmental costs. Decoupling solar energy supply from sunlight availability remains a major challenge for sustainable solar energy consumption. Delayed solar energy utilization in the dark was first developed by Fujishima et al. for anticorrosion applications with TiO_2@WO_3[1]. V_2O_5, $Ni(OH)_2$, WO_3, and ZnO were subsequently investigated for multi-photoelectron storage because of their diverse chemical states, which can reduce O_2 for bactericidal disinfection, heavy-metal reductions, or leave oxidative holes for pollutant degradations in dark[2-4]. Photocatalytic hydrogen evolution offers us the possibility to use green hydrogen for fuels and industrial applications. However, accompanied by energy loss during charge accumulation, that stored photoelectron rarely has sufficient redox potential for hydrogen generation in the dark.

Dark photosynthesis emerged as a promising strategy for controlled hydrogen production independent of sunlight since a few pioneering research works from Lotsch et al. They stored reducing radicals on long-lived photo-induced states in modified carbon nitride under irradiation, and then released them into hydrogen when coupled with an electrocatalyst in the dark.[5, 6] It establishes a new concept for releasing solar hydrogen on demand. During dark photosynthesis processes, multi-photoelectron storage is believed to be the key to hydrogen release. Based on previous findings that ruthenium(ii) dimer can store up to four electrons in ligands[7], Schulz et.al. achieved light harvesting and storage on a Cu(I) 4H-imidazolate complex and proposed a proton-coupled electron transfer mechanism, extending the charge storage for 14 h to

THE BIGGER PICTURE

Storing excess photon energy for the subsequent use in the dark represents a decoupled solar energy utilization strategy, resembling the dark reduction process in natural photosynthesis. This work demonstrates a promising strategy for decoupled hydrogen production from methanol-reforming, which represents a more feasible and efficient way for solar energy utilization. It may deal with the existing dilemma of low-efficiency photocatalytic reactions, including CO_2 reduction, N_2 fixation, CH_4 conversion etc. and on-demand solar energy utilization under intermittent sunlight. It further encourages human beings to learn from the nature in photosynthesis.

[1] These authors contributed equally to this work

[2] lead contact

[a] School of Materials Science and Engineering, Southeast University, Nanjing, 211189, P. R. China.

[b] SINOPEC (Beijing) Research Institute of Chemical Industry Co. Ltd, Beijing,100029, P. R. China.

[C] Department of Chemical Engineering, Tsinghua University, Beijing, 100085, P. R. China.

ruanqs@seu.edu.cn; jcr.bjhy@sinopec.com; zmsun@seu.edu.cn

cope with the day/night cycle[8]. Recently, Streb, Rau and Dietzek-Ivanšić et al. realized two photoelectrons storage in a single covalent photosensitizer–polyoxometalate (PS-POM) dyad molecular[9]. 2.5 h after the irradiation, the addition of a proton donor led to the instantaneous evolution of H_2. They achieved multi-electron storage, visible-light absorption, charge separation, and hydrogen release in a purely molecular photochemical device. Although comprehensive studies on dark photosynthesis focus on the prolonged lifetime of accumulated electrons, the energy loss of the stored photoelectron is scarcely investigated but is vital in hydrogen release. In a TiO_2-Cu_2O junction, multielectron trapping in an intermediate band between conduction bands (CBs) of TiO_2 and Cu_2O was found to be active for hydrogen release[10]. However, those trapped electrons were superficially attributed to a large potential difference between the CBs of TiO_2 and Cu_2O. For dark solar hydrogen production, an in-depth understanding of the energy loss of photoelectrons in charge accumulation and strategies to minimize the energy loss are highly demanded.

Very recently, path-breaking work from Luo et al. demonstrates a faradaic junction at TiO_2/CdS semiconductor/semiconductor interface[11]. A faradaic junction does not resemble the classic band-alignment process which is usually seen in physical junctions (such as Schottky junctions[12], p-n junctions[13], or Z-scheme junctions[14]) by showing a chemical redox reaction at the interface when photo-charges transfer across. In such a faradaic junction, isoenergetic charge transfer at the interface occurs via a reversible redox reaction of $Ti^{+4}O_{2-x}(OH)_{2x}$ /$Ti^{+3}O_{1-x}(OH)_{2x+1}$[11]. The isoenergetic charge transfer mechanism describes that high-energy photoelectrons can be stored in the form of photoredox chemicals at semiconductor-semiconductor junctions, that experience negligible redox potential loss despite the CB variations. The isoenergetic charge transfer in faradaic junctions was verified in several semiconductor junctions such as Si/WO_3, CoPi/$BiVO_4$, Fe_2O_3/$Ni(OH)_2$ and generated a series of solar rechargeable devices[15-22]. This theory of preserving high-energy photoelectrons at faradaic-junction interfaces should have great potential for solar hydrogen dark photosynthesis.

Building on these concepts, here we design and develop a TiO_x/CN faradaic junction for photoelectron storage and gradual release through a quasi-isoenergetic charge transfer process under irradiation, that achieves subsequent highly efficient hydrogen release from alkaline methanol in a dark condition for the first time. This TiO_x/CN junction photocatalyst produces a remarkable dark hydrogen yield of **2.4 mmol/g** from alkaline methanol within 0.5 h after turning off irradiation. Alkaline methanol reforming reaction is exothermal (negative enthalpy)[23], therefore, is favorable for hydrogen release even though the proton concentration is extremely small. Also, methanol acts as both the proton source and the hole scavenger. Deprotonation of methanol would enhance the proton concentration around the catalysts for easier hydrogen generation. The alkaline environment would benefit the storage of photoelectrons because proton donors would trigger photoelectron release into hydrogen in the presence of co-catalyst such as Pt.[6, 9] Isotope-labeling experiments, time-of-flight secondary-ion mass spectrometry (TOF-SIMS), and density functional theory (DFT) calculation show the origin and formation pathway of dark-released hydrogen. In-situ X-ray photoelectron spectroscopy (XPS), quasi-in-situ UV-Vis absorption, quasi-in-situ electron paramagnetic resonance (ESR), and photoelectrochemical techniques, etc. elucidated the quasi-isoenergetic charge transfer, storage and release process, which distinguished this faradaic junction from Z-scheme and type II heterojunctions. This work demonstrates the feasibility of a faradaic junction for highly efficient hydrogen synthesis after irradiation, which may potentially deal with the existing dilemma of solar energy utilization under intermittent sunlight.

RESULTS AND DISCUSSION

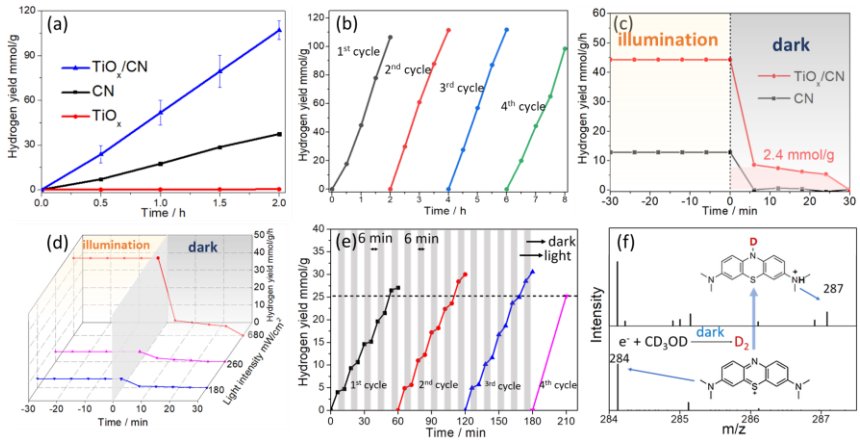

Figure 1. a) Hydrogen evolution of CN, TiO_x, and TiO_x/CN loaded with 3 wt% Pt under full arc illumination (300 W, Xenon lamp), b) cycling test of Pt loaded TiO_x/CN sample under illumination (4 cycles are presented as 1st, 2nd, 3rd, 4th cycle), c) dark hydrogen release of TiO_x/CN and CN loaded with 3 wt% Pt, d) dark hydrogen release of Pt loaded TiO_x/CN upon various light intensity (intensity: 680, 260, and 180 mW/cm^2), e) hydrogen generation of TiO_x/CN loaded with 3 wt% Pt under intermittent illumination (switching on/off light per 6 min, 1st, 2nd, 3rd cycle) and continuous illumination (4th cycle), f) Isotope labeling experiment: Methanol-D4 (CD_3OD) was added into the reactor after the light was turned off, and the resulting D_2 generated from CD_3OD in the dark was captured with methylene blue and detected by mass spectrometry (MS).

MXene (d-Ti_3C_2, a two-dimensional transition metal carbide) was chosen as the precursor of TiO_x because MXene is a two-dimension material that can be well-exfoliated and dispersed on the substrate after oxidation in the form of nano-particles.[24] Since MXene has variable valences (Ti^{2+}-Ti^{4+}), MXene oxidation products may also present variable valances in the presence of reductive photoelectrons, therefore, is beneficial to photoelectron storage. The preparation of MAX (Ti_3AlC_2, a polycrystalline nanolaminate of ternary carbides and nitrides) as a precursor of MXene and MXene was detailed in the experimental section, and XRD patterns confirmed their crystal structures in Figure S1. TiO_x/CN faradaic junction was synthesized via loading MXene on polymeric carbon nitride (CN), followed by in-situ oxidation by H_2O_2 in an ice-water bath. The crystal structure and light absorption properties of CN, TiO_x, and TiO_x/CN samples are shown and analyzed in Figure S2. XPS Ti 2p and O 1s spectra and the Raman spectrum in Figure S3 showed more structural details of TiO_x. The Ti 2p XPS spectrum showed two predominant Ti $2p_{3/2}$ and Ti $2p_{1/2}$ peaks at 458.8 and 464.7 eV, which could be further divided into four subpeaks corresponding to Ti^{3+} $2p_{3/2}$, Ti^{4+} $2p_{3/2}$, Ti^{3+} $2p_{1/2}$, and Ti^{4+} $2p_{1/2}$, respectively.[25] The binding energies (529.3 eV, 530.7 eV, and 532.0 eV) of O 1 s are observed in Figure S3b and assigned to the lattice O^{2-}, lattice OH^-, and adsorbed H_2O molecules.[11] The presence of lattice OH^- confirms a $TiO_{x-1}(OH)$ layer on the surface of TiO_x. Raman spectrum of TiO_x in Figure S3c showed the rutile structure[11], however, due to abundant surface hydroxyl groups, the crystallinity of TiO_x is rather low. CN in TiO_x/CN was characterized by FTIR, ^{13}C NMR, and XPS spectra in Figure S4, confirming its polymeric carbon nitride structure.[26]

CN, TiO_x, and TiO_x/CN powders have been photo-deposited with 3 wt% Pt and measured for photocatalytic hydrogen generation from alkaline methanol under illumination in an inert atmosphere. All samples tested in Figure 1 have been preloaded with 3 wt% Pt unless otherwise stated. As a control experiment, TiO_x did not show any solar hydrogen activity in Figure 1a. TiO_x/CN exhibits a hydrogen yield of 51.7±8.5 mmol/h/g, which is 3 times of pure CN (17.4 mmol/h/g). The cycling test of Pt-loaded TiO_x/CN in Figure 1b confirmed its good stability. Delayed solar hydrogen generation rates for TiO_x/CN and CN were monitored in the dark in Figure 1c. Within

0.5 h after the illumination, TiO_x/CN showed an outstanding hydrogen yield of 2.4 mmol/g in the dark (the integral of hydrogen production rate over time derived from the red region in Figure 1c). Roughly 20% excited electrons can be used for dark hydrogen release on TiO_x/CN junction as the hydrogen yield deceased from 45 mmol/g/h under illumination to ca. 10 mmol/g/h in the dark. To show the extraordinary performance, a video was recorded under the illumination of a 300 W Xenon lamp and after turning off the illumination (Supplementary information). A summary of dark hydrogen production over various photocatalysts have been displayed in Table S1 although absolute comparison between photocatalysts is not applicable as the performance may also depend on illumination geometry, light source, illumination duration, reactors etc. As a control experiment, CN showed negligible hydrogen release in dark, suggesting its poor photoelectron accumulation ability. Varying the light intensity from 680 mW/cm^2 to 180 mW/cm^2 resulted in a decrease in the total dark hydrogen yield over TiO_x/CN from 2.4 mmol/g to 0.4 mmol/g as shown in Figure 1d, suggesting that dark hydrogen release was affected by the photoelectrons accumulation under illumination through a light-intensity-dependent dynamic equilibrium. This dynamic equilibrium can be likened to the accumulating and releasing of photoelectrons.

In Figure 1e, we stimulated a short-cycle intermittent irradiation condition in nature by switching on/off light per 6 min. There is sample activation in the 1st cycle and the activity became stable for the 2nd and 3rd cycles. For 60 mins intermittent irradiation (30 min illumination, 30 min dark), the junction evolved 29.2±2.1 mmol/g hydrogen on average, which is 16% more efficient than continuous irradiation for 30 mins (purple line; hydrogen yield: 25.2 mmol/g). It indicates that this faradaic junction could store photoelectrons, which would have been wasted in continuous irradiation, for the following dark photosynthesis. Isotope-labeling experiments were performed to confirm the generation of hydrogen in the dark as shown in Figure 1f. The Pt-preloaded TiO_x/CN was initially suspended in alkaline CH_3OH under illumination. Immediately after turning off the light, CD_3OD was injected into the airtight reactor. The dark synthesized D_2 was captured using a solution of colloidal platinum in methylene blue (MB, $C_{16}H_{18}N_3S^+$, m/z=284) to form leucoMB ($C_{16}H_{19}N_3SD^+$, m/z = 287)[27]. The transition from $C_{16}H_{18}N_3S^+$ to $C_{16}H_{19}N_3SD^+$ was identified by mass spectrometry in Figure 1f, validating the generation of HD or D_2 from CD_3OD in the dark by pre-stored photoelectrons. It is worth noticing that NaOH may also act as a proton source in alkaline methanol reforming (Methanol photo-oxidation: $CH_3OH + 6h^+ + 2OH^- \rightarrow CO_3^{2-} + 6H^+$; Proton reduction: $6H^+ + 6e^+ \rightarrow 3H_2$).[23]

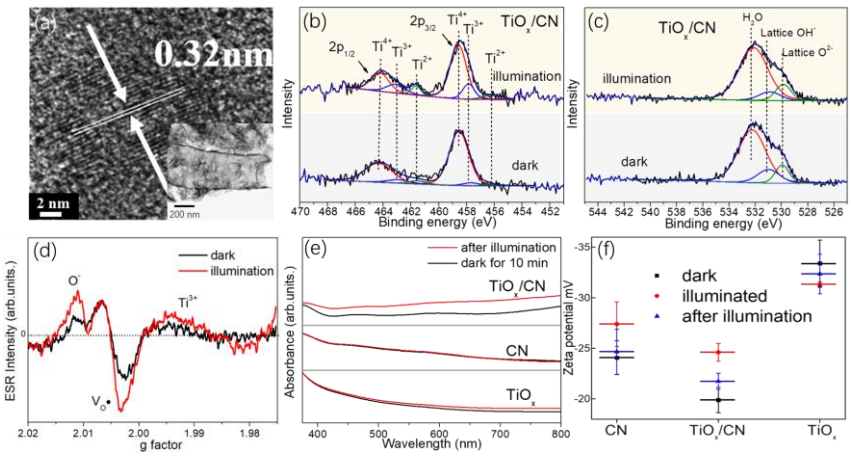

Figure 2. a) TEM lattice spacing of TiO_x/CN (inset: images of TiO_x nanoparticles on CN); In-situ XPS b) Ti 2P and c) O 1s spectra of TiO_x/CN in dark and under illumination; d) quasi-in-situ ESR spectra of TiO_x/CN before and immediately after illumination; e) quasi in-situ UV-Vis absorbance of TiO_x, CN and TiO_x/CN right after illumination and leaving in the dark for 10 mins; f) ex-situ Zeta potential of TiO_x, CN and TiO_x/CN under different illumination conditions.

The lattice spacing of TiO_x nanoparticles on CN is 0.32 nm in Figure 2a corresponding to the (110) crystal plane of rutile[11]. However, due to its small particle

size and abundant surface hydroxyl groups, the crystallinity of TiO_x is rather low. Figure 2a (inset) displays the TEM images of the TiO_x/CN junction. The corresponding Ti, C, N, and O elements mapping in Figure S5 fit the shape of particles, suggesting the loading of TiO_x on CN nanotubes. To differentiate the faradaic junction from the type II heterojunction and the Z-scheme heterojunction, photoelectron transfer conditions were investigated. TiO_x and TiO_x/CN junction were characterized by in-situ XPS under illumination in Figures 2b and c. Under illumination, TiO_x showed a negligible shift in Ti 2p binding energy compared to its ground state (dark condition) in Figure S6, suggesting that photoelectron accumulation is difficult in the single TiO_x material. For TiO_x/CN junction, both Ti $2P_{3/2}$ and Ti $2P_{1/2}$ experienced an obvious shift to lower binding energy (458.8 eV to 458.5 eV, 464.7 eV to 464.4 eV). As a result, peaks attributed to Ti^{3+} $2p_{3/2}$ (457.6 eV), Ti^{3+} $2p_{1/2}$ (463.2 eV), Ti^{2+} $2p_{3/2}$ (456.1 eV), and Ti^{2+} $2p_{1/2}$ (461.7 eV) arise upon illumination[24], indicating a conversion from Ti^{4+} to Ti^{3+} and Ti^{2+} upon photoelectron injection from CN. It suggests that photoelectrons can be stored in a form of Ti^{3+} or Ti^{2+} and hence TiO_x/CN junction is not a Z-scheme heterojunction where holes in CN recombined with electrons in TiO_x as illustrated in Figure S7, leaving electrons on CN. In TiO_x/CN, illumination also increased the proportion of lattice O^{2-} and decrease the lattice OH^- as shown in XPS O 1s spectra (Figure 2c) due to the hole oxidation of lattice OH^-. C 1s and N 1s XPS spectra show no obvious change before and under illumination in Figure S8, suggesting that CN only supplied photoelectrons but did not store them. It is worth noticing that there are previous reports on terminal groups modified polymeric carbon nitride can store photoelectrons[5, 6], however, such photoelectron storage terminals were excluded by Fourier Transform Infrared Spectrometer (FTIR) and ^{13}C Nuclear magnetic resonance (NMR) spectra in our CN or TiO_x/CN in Figure S9.

To investigate the change of TiO_x and CN in photo-electron accumulation, photo-induced vacancies in TiO_x/CN upon illumination were investigated by quasi-in-situ ESR in Figure 2e. An intensive ESR signal (g = 2.004) was observed in dark, representing single-electron-trapped oxygen vacancy ($V_o^{\bullet}$) due to the presence of Ti^{3+} in TiO_x[28]. The red line indicates the ESR spectrum upon light illumination, which can be split into three signals with g factors of 1.988, 2.004, and 2.010 as illustrated in Figures 2d and S10. The enhanced signal of $V_o^{\bullet}$ under illumination was due to the presence of more Ti^{3+} by electron injection, which is accompanied by an enhancement of the Ti^{3+} signal at g=1.988 upon illumination.[29] A new signal (g=2.010) emerged as a result of surface O^- species generated from the interaction of O_2 with the photoinduced surface Ti^{3+} species[30]. As a comparison, CN showed the same ESR signal (g=2.003) before/after illumination in Figure S11, suggesting that no photoinduced vacancies occurred, that is no photoelectron storage on CN.

Quasi-in-situ UV/Vis was applied to further verify the photoelectron accumulation on Ti sites at the TiO_x and CN interface. TiO_x, CN, and TiO_x/CN were deposited on the FTO substrate and illuminated in 0.1 M Na_2S aqueous solution. With hole scavengers (0.1 M Na_2S), the UV-Vis absorbances of three films were collected right after the light was turned off and after 10 minutes in the dark, respectively. The comparisons were shown in Figure 2e. TiO_x exhibits higher light absorbance upon illumination, which has been interpreted as photoelectron storage in the space charge layer with the reduction of Ti^{+4} to Ti^{+3}.[31] The broad absorption band at 400–800 nm likely arises from the metal-to-metal intervalence transitions.[32] The more prominent absorbance enhancement of TiO_x/CN after illumination, therefore, verified the electron accumulation on Ti^{+3} atoms at TiO_x/CN interface after photoelectron transferring from CN. As a control, CN has shown a negligible change of absorbance upon illumination. Such a charge accumulation behavior on TiO_x/CN sample distinguished the faradaic junction from the type II junction.

Moreover, the photo-electron accumulation condition is investigated by ex-situ Zeta potential measurements. In Figure 2f, TiO_x/CN showed a negative Zeta potential of -19.88±1.25 mV, which changes to -24.6±0.88 mV right after UV irradiation. The more negative zeta potential is due to the formation of hydrophilic reducing chemicals in a faradaic junction that might be TiO_xH_y. 10 mins after the illumination, the suspension recovered the zeta potential to -21.73±0.80 mV due to partial reoxidation of TiO_xH_y. In Figure 2f, the change of Zeta potential on irradiation conditions for CN or TiO_x is less prominent. Therefore, the photoelectron accumulation ability of TiO_x/CN faradaic junction outweighs single CN or TiO_x. The Zeta potential change of CN is probably due to the change of its space charge layer. (Photogenerated holes diffuse to the surface along the upward band bending, resulting in the absorbance of hydroxyl groups on the surface.[33] Therefore, the zeta potential became more negative upon illumination.)

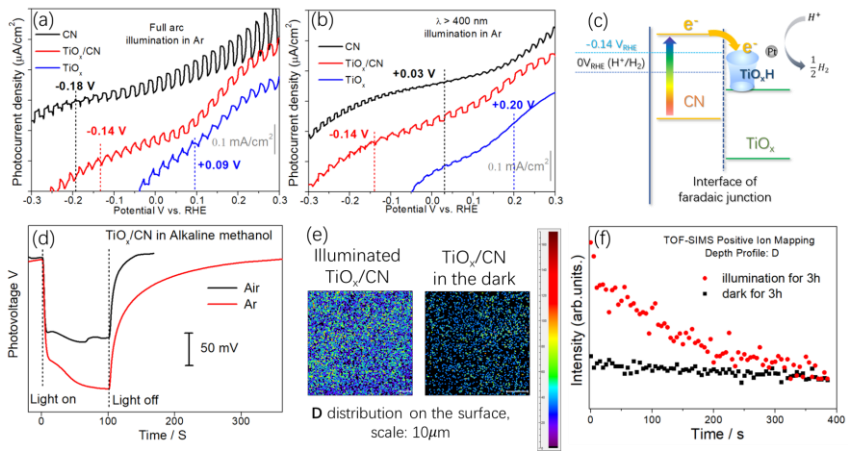

Figure 3. Photocurrent onset potentials of CN, TiO_x, and TiO_x/CN in argon atmosphere a) under full-arc illumination and b) under visible-light illumination (λ>400 nm), (photocurrent densities of CN, TiO_x/CN and TiO_x have been amplified by 5, 2 and 10 times, electrolyte: 1M Na_2S aqueous solution); c) schematic of electron storage and transfer at the interface of TiO_x/CN faradaic junction; d) photovoltage of TiO_x/CN in alkaline methanol in argon and air, e) TOF-SIMS positive ion mapping for D on the surface of TiO_x/CN films immersed in methanol-D4 with and without illumination, f) depth profile of secondary ion intensities of D for TiO_x/CN in methanol-D4 with and without illumination.

Apart from the photoelectron accumulation ability, the TiO_x/CN faradaic junction is different from the type II heterojunction because of its (quasi)-isoenergetic charge transfer feature. Therefore, we investigate the charge transfer process in TiO_x/CN faradaic junction through photoelectrochemical methods. The intimate contact between TiO_x and CN was proved by photocurrent vs. time plots under chopped light and Electrochemical impedance spectroscopy (EIS) in Figure S12. The band structures of TiO_x and CN were determined by Ultra-Violet Photoelectron Spectroscopy (UPS) in Figure S13. The conduction band (CB) position of TiO_x is +0.1 V_{RHE}, which is insufficient for hydrogen evolution, agreeing with its negligible hydrogen evolution rate as shown in Figure 1a. The CB of CN is determined to be -1.0 V_{RHE}. The photocurrent onset potential of CN and TiO_x, at which the inversion between cathodic and anodic photocurrents occurs in chopped LSV plots in argon atmosphere [34], located at -0.18 V_{RHE} and +0.09 V_{RHE} under full-arc illumination in Figure 3a, respectively, representing the flat-band potentials of materials. The flat-band potential of TiO_x agrees with its conduction band, while that of CN is roughly 0.8 V lower than its conduction band due to abundant surface terminal states as shown in Figure S4c,

d.[35] Under full-arc illumination, TiO_x/CN exhibited a slightly lower onset potential of -0.14 V_{RHE} compared to CN (-0.18 V_{RHE}), indicating that photoelectrons experienced only a small potential drop when transferred at the junction interface.

As a comparison, TiO_x, CN, and TiO_x/CN photoelectrodes were tested in argon under visible-light illumination (λ>400 nm) in Figure 3b. Under visible-light illumination, TiO_x exhibits negligible photocurrent response, suggesting defect-induced charge recombination dominates under visible light. The onset potential of CN positively shifted to +0.03 V_{RHE} under visible light compared to that under full-arc illumination, suggesting the energy of excited electrons depreciated under visible light.[34] However, TiO_x/CN maintained the same onset potential of -0.14 V_{RHE} under visible illumination as that under full-arc illumination suggesting that energy levels of photoelectrons do not depreciate under visible-light, which is explained by photoelectrons storage at TiO_x/CN junction through an quasi-isoenergetic charge transfer. Such a quasi-isoenergetic charge transfer not only maintained the energy of photoelectrons but also improved photocurrent density by helping charge separation, which is verified by the enhanced hydrogen performance in Figure 1a. As a result, TiO_x/CN still showed hydrogen generation in the dark (Figure S14), although TiO_x showed no photo-response under visible-light illumination. For a type II heterojunction, if most TiO_x is attached to the FTO substrate, photoelectrons transferred from CN to TiO_x should fall on the CB of TiO_x, showing an onset potential around +0.10 V_{RHE}.[36] Under visible-light illumination, if most CN attached the FTO, the onset-potential of TiO_x/CN should follow the onset potential of CN, that is +0.03 V_{RHE}. Therefore, the maintained onset potential (-0.14 V_{RHE}) of TiO_x/CN under visible-light illumination verified the quasi-isoenergetic charge transfer at TiO_x and CN interface rather than a type II heterojunction. The mechanism of photocatalysis on faradaic junctions was illustrated in Figure 1c. Photoelectrons excited to the CB of CN were iso-energetically transferred and accumulated at the CN and TiO_x interfaces, which subsequently reduce protons into hydrogen in the dark.

To investigate the lifetime of (quasi)-isoenergetic electrons stored in a form of reducing chemicals for hydrogen release from alkaline methanol, we measured the Open circuit photovoltage (OCP) decay of TiO_x/CN in alkaline methanol with argon and air, respectively, in Figure 3d. In the argon atmosphere, TiO_x/CN experienced a very slow OCV decay over 200 s, suggesting that this faradaic junction can store quasi-isoenergetic photoelectrons and release them slowly in the dark. The decay of OCV can be due to stored photoelectrons consumed by electron scavengers such as protons or oxidative intermediate products in methanol reforming. For example, with oxygen, OCP decays within 20 s and the OCP is smaller than that in argon because oxygen as an electron scavenger prevents the photoelectron accumulation and accelerates its dark release as proved in Figure S15. The reducing chemical for photoelectron storing at the TiO_x/CN faradaic junction interface is crucial, whose elemental composition was therefore investigated by time-of-flight secondary-ion mass spectrometry (TOF-SIMS). TiO_x/CN was compressed into films and immersed in methanol-D4 for 3 h in the dark or under illumination. The D element mapping on the surface was shown in Figure 3e. The ion intensity of D is significantly stronger for the illuminated sample than that in the dark, suggesting the formation of TiO_xHD under illumination. However, the surface of Ti is hydroxylated (generally H-containing) and the weakly bound H^+ may be exchanged by D^+ in methanol-D4.[37] Therefore, we sputtered the surface of TiO_x/CN with an ion gun for 400 s to get a depth profile of D ion in Figure 3f. The D ion intensity decreases with depth for the illuminated sample but remained almost constant for the sample in the dark. It indicates that D ion can penetrate the surface and react with TiO_x under illumination rather than exchanged

with surface H^+. Since D is derived from methanol-D4, TiO_xHD is, therefore, the reducing chemical for quasi-isoenergetic photoelectron accumulation.

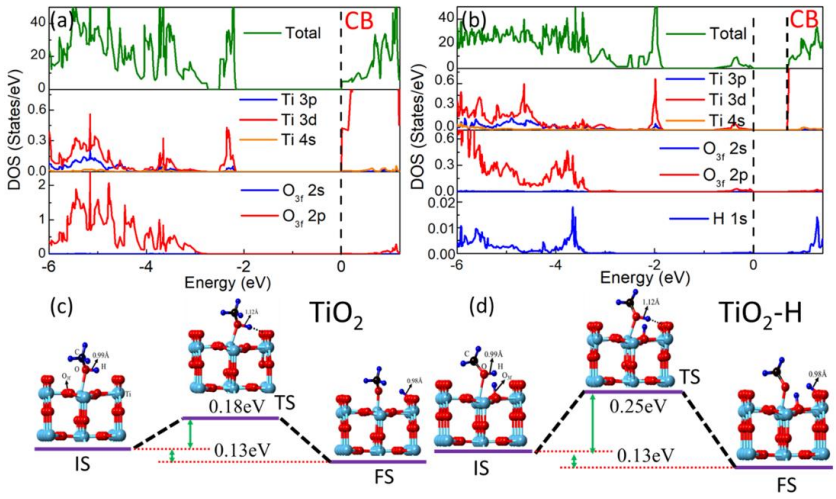

Figure 4. The total and partial density of states DOS of a) rutile TiO_2 (110) surface and b) TiO_2 (110)-H surface; the energy of methanol dissociation on c) TiO_2 and d) TiO_2-H, (blue atom is H, the red atom is O, the black atom is C, light blue atom is Ti).

To understand the mechanism behind (quasi)-isoenergetic photoelectron accumulation and release processes of a TiO_x/CN faradaic junction, a DFT calculation was carried out. In Figure 4, a hydrogen atom was added onto the surface of rutile TiO_2, to stimulate the reducing chemical TiO_xH_y at the interface of a faradaic junction. In Figure 4a, b, the addition of the H atom lifts the CB of TiO_2 (e.g., by 0.6 eV) for photoelectron accommodation at higher energy levels, reducing the energy loss of a photoelectron transferring from CN. This results in the (quasi)-isoenergetic photoelectron accumulation. Regarding the release of accumulated photoelectrons, we evaluated the feasibility of methanol dissociation on the TiO_2 surface with/without H addition in Figure 4c, d. With a surface H atom, the methanol dissociation energy difference between the initial state (IS) and transition state (TS) increased, e.g., from 0.18 eV (TiO_2) to 0.25 eV (TiO_2-H). It suggests that photoelectrons stored in the form of TiO_xH_y have difficulties in directly grasping the H atom from methanol for the following hydrogen release. This can be explained by the repulsion force between electron clouds of adjacent hydrogen atoms as illustrated in Figure S16. Thus, the hydrogen release process is likely due to the reverse redox reaction between TiO_x and TiO_xH_y, during which the electron was released and proceeded the following proton reduction.

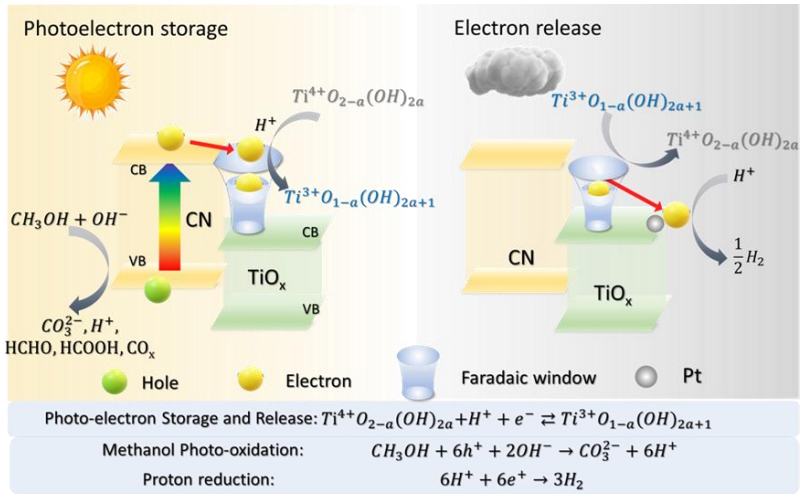

Scheme 1. Photoelectron storage and release scheme in a faradaic junction for decoupled solar hydrogen production from alkaline methanol. To be precise, TiO_x was represented by $TiO_{2-a}(OH)_{2a}$, and TiO_xH_y was represented by $TiO_{1-a}(OH)_{2a+1}$.

To understand the photoelectron release pathway, the location of Pt on TiO_x/CN as a co-catalyst was investigated before and after the reaction in Figure S17. Pt shows two prominent peaks at 71.05 eV and 72.15 eV referring to Pt^0 and Pt^{2+}, respectively. Loading Pt also shifts the O 1s peak to lower binding energy, suggesting the existence of PtO_x. After depositing Pt on TiO_x/CN, XPS spectra of Ti 2p experienced a 0.4 eV shift to lower binding energy, indicating the injection of electrons from Pt to TiO_x. Combining with the Pt mapping of Pt-TiO_x/CN in Figure S18, we can conclude that Pt atoms were loaded on both TiO_x and CN in TiO_x/CN sample. Therefore, the release of stored electrons from TiO_xH may directly transfer to adjacent Pt active sites for proton reduction reaction. After 3h reaction, no obvious change was observed for C 1s, N 1s, and Ti 2p spectra, suggesting the stability of this photocatalyst, while Pt^0 was partially oxidized after reaction probably due to formation of $\mathrm{Pt-(OH)_{ads}}$ intermediates in alkaline condition following $\mathrm{Pt + OH^- \rightarrow Pt-(OH)_{ads} + e^-}$.[38, 39]

Finally, we described the scheme of photoelectron storage and gradual release for delayed solar hydrogen production from alkaline methanol in Scheme 1. Upon sunlight irradiation, photoelectrons are lifted to the CB of CN, leaving holes to oxidize methanol into CO_3^{2-} and release H^+. Photoelectron storage occurs at the TiO_x/CN interface, where electrons flow from CN reduced $Ti^{4+}O_{2-a}(OH)_{2a}$ into $Ti^{3+}O_{1-a}(OH)_{2a+1}$ in the presence of H^+. The redox potential of $Ti^{4+}O_{2-a}(OH)_{2a}/Ti^{3+}O_{1-a}(OH)_{2a+1}$ is more negative than H_2/H^+ redox potential) due to a quasi-isoenergetic electron transfer process. A window of this faradaic junction is the gap between $Ti^{4+}O_{2-a}(OH)_{2a}/Ti^{3+}O_{1-a}(OH)_{2a+1}$ redox potential and the CB of TiO_x, where charge accumulation can occur. This distinguishes the TiO_x/CN faradaic junction from the type II and Z-scheme heterojunction. The reversible redox reaction between $Ti^{4+}O_{2-a}(OH)_{2a}/Ti^{3+}O_{1-a}(OH)_{2a+1}$ releases high-energy electrons that further reduce H^+ into hydrogen without illumination. The photoelectron storage process at the faradaic junction interface stores excessive photoelectrons and delays the release of solar hydrogen, thereby decoupling the photocatalytic hydrogen evolution from immediate sunlight irradiation and improving the efficiency of photocatalysis.

Methanol reforming involves many other intermediate products apart from CO_2 (Figure S19). The current doubling effect is an important phenomenon in methanol oxidation, especially on titanium oxide species[40, 41] Current Doubling effect is the current multiplication due to the formation of unstable $\bullet CH_2OH$ radicals followed by electron injection into the conduction band of a photocatalyst in a photoelectrochemical cell functioning in the presence of methanol[42]. The current doubling effect leads to additional electron injection into the TiO_x/CN faradaic junction in our work, which can be a part of the source of stored electrons. At this stage, it is difficult to distinguish additional electrons released by radicals from photogenerated electrons, however, it would be interesting to explore the impact of the current doubling effect on electron storage in the future.

CONCLUSION

In summary, this study reports photoelectrons stored in a TiO_x/CN faradaic junction for highly efficient solar hydrogen release in the dark from alkaline methanol. The delayed utilization of photoelectrons at the interface of TiO_x/CN is a result of the accumulation and gradual release of quasi-isoenergetic photoelectrons, characterized by in-situ XPS, quasi-in-situ UV-Vis absorption, quasi-in-situ ESR, and photoelectrochemical techniques, etc. Isotope experiment and TOF-SIMS confirmed that those photoelectrons are stored in a form of reducing chemicals (TiO_xH_y) in the absence of oxygen. DFT calculations revealed that those stored photoelectrons are inactive to methanol, but they can gradually release active electrons for proton reduction into hydrogen in the dark. This study, therefore, demonstrates a promising strategy for temporally decoupling sunlight and the efficient release of hydrogen. It may potentially overcome the dilemma of solar energy utilization under intermittent sunlight.

EXPERIMENTAL PROCEDURES

Preparation of TiO_x

Firstly, MAX (Ti_3AlC_2) was synthesized by pressureless sinterin[43]. TiC (2-4 μm, 99%, Aladdin), Al (300 mesh, 99.7%, ZhongNuo Advanced Material), and Ti (300 mesh, 99.99%, Aladdin) were mixed in a powder mixer at a molar ratio of 1.8:1:1 for 24 h. The mixed powder was placed in an alumina crucible in a tubular furnace (KeJin, GSL-17800X) in the argon under the condition of temperature increasing to 1450 ℃ at a heating rate of 10 ℃/min and held for 2 h, the mass Ti_3AlC_2 was collected after naturally cooling. Ti_3AlC_2 powder was obtained through vibration crushing, mechanical grinding, and 300 mesh sieving. XRD pattern of MAX(Ti_3AlC_2) is shown in Figure S1.

Then, MXene (Ti_3C_2) was prepared by etching the Ti_3AlC_2 powder using LiF (AR, 99%, Aladdin)/HCl (AR, 38%, Sinopharm) solution. In detail, 2.0 g of Ti_3AlC_2 powder was slowly added into LiF/HCl solution (2.0 g LiF dispersed into 40 mL of 12 M HCl), which was continuously stirred for 24 h at 40 ℃. Afterward, the turbid suspension was centrifuged to collect the precipitate, followed by washing it with deionized water several times until the pH turned neutral. The precipitates were further rinsed with ethanol three times before vacuum-drying at 80℃ for 12 h, resulting in multilayered Ti_3C_2. Then 2.0 g of multilayered Ti_3C_2 was dispersed into 100 mL of deionized water, followed by ultrasonication in an ice-water bath for 1 h. The dispersion was centrifugalized at 3500 rpm for 1 h[44]. Finally, Ti_3C_2 was collected from the supernatant. XRD pattern of MXene (Ti_3C_2) is shown in Figure S1.

10 mL of 3.0 wt% H_2O_2 (AR, 30 wt%, Aladdin) was dropwise added into 100 mL of 2.0 mg/mL $Ti_3C_2T_x$ suspension under vigorous stirring in an ice-water bath. The mixture was kept vigorously stirring for 10 min and subsequently immersed in liquid nitrogen. After the dispersion was completely frozen, it was subjected to a vacuum freeze drier for at least 24 h. The obtained powder was labeled as TiO_x.

Preparation of CN

The carbon nitride (CN) was prepared by calcining the mixture of urea (99.5%, Aladdin) and melamine (99%, Aladdin) at the mass ratio of 12:1 in a cylindrical crucible with a cover in a muffle furnace (Boyuntong, KF1200) in the air. The temperature was increased room temperature to 180 ℃ at a heating rate of 2.5 ℃/min and hold for 30 min, followed by heating to 550 ℃ at a rate of 2.5 ℃/min and keeping for 120 min. After cooling, the material was obtained and labeled as CN.

Preparation of TiO_x/CN faradaic junction

50 mg CN was dispersed into 25 mL of deionized water, followed by ultrasonication for 0.5 h. And 5 mL of 2.0 mg/mL $Ti_3C_2T_x$ MXene nanosheet solution was dropwise added into the CN suspension under vigorous stirring for 2 h in an ice-water bath. And 2.5 mL of 3.0 wt% H_2O_2 was dropwise added into suspension under vigorous stirring for 10 min, then subsequently immersed in liquid nitrogen. After completely frozen, the suspension was subjected to a vacuum freeze drier for at least 24 h, which was labeled as TiO_x/CN.

Preparation of CN, TiO_x, TiO_x/CN photoelectrodes

1 mg sample was dispersed in 10 mL of deionized water with the addition of 10 μL Nafion (Aladdin), followed by ultrasonication for 0.5 h. Whereafter, 250 μL

suspension was dropped onto 2cm x 2cm Fluorine Doped Tin Oxide (FTO) substrate and was dried at 80℃.

Characterizations

SEM/TEM (FEI, Sirion)/(Thermal Fisher, Talos F200X) was used to take morphology images of CN, TiO_x, and TiO_x/CN. **XRD** (HaoYuan, D8-Discover) was used to analyze and characterize the crystal structure of the sample, equipped with a Cu target. **UV-Vis** (SHIMADZU, UV-2600) was used to characterize the optical absorption performance of the sample in a wavelength range of 300-800 nm. **In-situ XPS** (PHI-Vesoprobe 5000 Ⅲ) was used to monitor the chemical states of Ti and O elementals in dark and under illumination, respectively. A xenon lamp was used as the illumination source during the test. **Electron Paramagnetic Resonance Spectrometer** (ESR, Bruker EMX PLUS) was used to investigate the O vacancies of TiO_x/CN and CN before and after the illumination. Firstly, TiO_x/CN and CN were tested in the dark. Data were collected again after 10 mins of illumination (Xenon lamp). **Zeta potential** (Nanobrook, Omni) was used to study the surface charge condition of samples. 10 mg CN, TiO_x, and TiO_x/CN samples were suspended in 10 mL water by sonicating for 10 mins. 2 mL supernatant was transferred into a quartz cuvette. The supernatant was stabilized for 5 mins before the test. After that, the supernatant was illuminated with a 300 W Xenon lamp for 10 min and then tested immediately. Finally, the supernatant was placed in the dark for another 10 min and tested for the third time. **Time-of-flight secondary-ion mass spectrometry** (PHI nanoTOF II Time-of-Flight SIMS) was used to investigate the elemental composition beneath the surface. The ion species is Ar ion, with an energy of 3 kV, 100 nA. The sputtering rate is 0.056 nm/s on SiO_2.

Performance tests

Hydrogen evolution test: The photocatalytic hydrogen evolution was tested in an airtight quartz reactor under a 300 W xenon lamp. The photocatalytic reactions were conducted at atmospheric pressure and room temperature. Typically, a 10 mg sample was per-loaded with 3 wt% Pt and mixed with 50 mL CH_3OH and 5 g NaOH in an airtight quartz reactor. The suspension was degassed by argon for 30 min. The hydrogen was analyzed by gas chromatograph (GC9790Plus, FuLi).

Isotope-labeling experiment: 5 mg TiO_x/CN was per-loaded with 3 wt% Pt and mixed with 10 mL CH_3OH and 1 g NaOH in an airtight quartz reactor. The reactor was illuminated with a 300 W Xenon lamp and the reactor was purged with argon until the light was turned off. 10 mL CD_3OD was then injected into the reactor via a syringe. The solution was placed in the dark for 30 mins to generate D_2. 100 μL colloidal platinum in methylene blue solution (miz, ENH-1000, Japan) was added into the reactor. 1 mL of the mixed solution was filtered and transferred into a glass bottle for mass spectrometry measurements in a Liquid-phase high-resolution time of Flight mass spectrometer (Agilent, 1260-6224)

Photoelectrochemical measurements: LSV plots were collected in 1 M Na_2S (pH=13.4) aqueous electrolyte. For measurements in oxygen-free conditions, the electrolyte was degassed with Ar for 10 mins before the test to remove dissolved oxygen. Photovoltage was collected under a 300 W Xenon lamp in alkaline methanol (6 g NaOH dissolved in 60 mL methanol) degassed electrolyte. It should be noted that using a pH meter to measure the pH value of alkaline methanol will introduce an error due to the different diffusivity of H^+ in methanol versus water. It is unreliable to adjust the potential in alkaline methanol to RHE, which is why we did not scale the potential drop for methanol electrolyte in the manuscript Figure 3d.

Density functional theory (DFT) calculation

All the first-principles calculations in this work were performed by using the Vienna ab initio simulation package (VASP), in which the interactions of core-electron were described by the projector augment wave (PAW) potentials and the exchange-correlation functional were modeled by PBE-GGA. A kinetic cut-off energy of 450 eV is used for the plane-wave basis set. The van der Waals (vdW) interaction is considered by adopting the DFT-D3 method (an empirical dispersion correction scheme of Grimme).

The rutile TiO_2 (110) surface was modeled by a 3 x 1 supercell of a three-layered slab model with a vacuum of 15 Å. Atoms in the bottom two layers were fixed and the top layers of the surface were allowed to relax. A 4 × 4 × 1 Monkhorst-Pack (MP) k-point sampling is adopted for structural optimizations using the conjugated gradient (CG) method with the convergence thresholds of 1×10^{-5} eV/atom for the total energy, 0.02 eV $Å^{-1}$ for the maximum force. The dissociation of methanol on the rutile TiO_2 （

110) surface was evaluated by using the climbing image nudged elastic band (CI-NEB) method.

SUPPLEMENTAL INFORMATION

Supplemental experimental procedures, Document S1. Figures S1–S19, and Table S1

Video S1. Hydrogen evolution under and after irradiation

ACKNOWLEDGMENTS

This work acknowledges financial support from the National Natural Science Foundation of China (NSFC) under Grant NO. 22102024

AUTHOR CONTRIBUTIONS

Q.R and X.X conducted the experiments and drafted the paper. C.J. and ZM.S. supervised the work. B.Y. conducted the DTF calculations, L.K. conducted the TEM. J.T. revised the manuscript.

DECLARATION OF INTERESTS

The authors declare no competing interests.

REFERENCES

1. Tatsuma, T.; Saitoh, S.; Ngaotrakanwiwat, P.; Ohko, Y.; Fujishima, A., Energy storage of TiO2– WO3 photocatalysis systems in the gas phase. *Langmuir* **2002,** *18* (21), 7777-7779.

2. Sakar, M.; Nguyen, C. C.; Vu, M. H.; Do, T. O., Materials and mechanisms of photo‐assisted chemical reactions under light and dark conditions: can day‐night photocatalysis be achieved? *ChemSusChem* **2018,** *11* (5), 809-820.

3. Liu, N.; Lu, N.; Yu, H.; Chen, S.; Quan, X., Efficient day-night photocatalysis performance of 2D/2D Ti3C2/Porous g-C3N4 nanolayers composite and its application in the degradation of organic pollutants. *Chemosphere* **2020,** *246*, 125760.

4. Takahashi, Y.; Tatsuma, T., Oxidative Energy Storage Ability of a TiO2– Ni (OH) 2 Bilayer Photocatalyst. *Langmuir* **2005,** *21* (26), 12357-12361.

5. Kröger, J.; Jiménez‐Solano, A.; Savasci, G.; Rovó, P.; Moudrakovski, I.; Küster, K.; Schlomberg, H.; Vignolo‐González, H. A.; Duppel, V.; Grunenberg, L., Interfacial engineering for improved photocatalysis in a charge storing 2D carbon nitride: melamine functionalized poly (heptazine imide). *Advanced Energy Materials* **2021,** *11* (6), 2003016.

6. Lau, V. W. h.; Klose, D.; Kasap, H.; Podjaski, F.; Pignié, M. C.; Reisner, E.; Jeschke, G.; Lotsch, B. V., Dark photocatalysis: storage of solar energy in carbon nitride for time‐delayed hydrogen generation. *Angewandte Chemie* **2017,** *129* (2), 525-529.

7. Konduri, R.; Ye, H.; MacDonnell, F. M.; Serroni, S.; Campagna, S.; Rajeshwar, K., Ruthenium photocatalysts capable of reversibly storing up to four electrons in a single acceptor ligand: A step closer to artificial photosynthesis. *Angewandte Chemie* **2002,** *114* (17), 3317-3319.

8. Schulz, M.; Hagmeyer, N.; Wehmeyer, F.; Lowe, G.; Rosenkranz, M.; Seidler, B.; Popov, A.; Streb, C.; Vos, J. G.; Dietzek, B., Photoinduced charge accumulation and prolonged multielectron storage for the separation of light and dark reaction. *Journal of the American Chemical Society* **2020,** *142* (37), 15722-15728.

9. Amthor, S.; Knoll, S.; Heiland, M.; Zedler, L.; Li, C.; Nauroozi, D.; Tobaschus, W.; Mengele, A. K.; Anjass, M.; Schubert, U. S., A photosensitizer–polyoxometalate dyad that enables the decoupling of light and dark reactions for delayed on-demand solar hydrogen production. *Nature Chemistry* **2022,** *14* (3), 321-327.

10. Yasomanee, J.; Bandara, J., Multi-electron storage of photoenergy using Cu2O–TiO2 thin film photocatalyst. *Solar Energy Materials and Solar Cells* **2008,** *92* (3), 348-352.

11. Chen, M.; Dong, H.; Xue, M.; Yang, C.; Wang, P.; Yang, Y.; Zhu, H.; Wu, C.; Yao, Y.; Luo, W., Faradaic junction and isoenergetic charge transfer mechanism on semiconductor/semiconductor interfaces. *Nature communications* **2021,** *12* (1), 1-8.

12. Xiao, Y.; Guo, S.; Tian, G.; Jiang, B.; Ren, Z.; Tian, C.; Li, W.; Fu, H., Synergetic enhancement of surface reactions and charge separation over holey C3N4/TiO2 2D heterojunctions. *Science Bulletin* **2021,** *66* (3), 275-283.

13. Tian, N.; Huang, H.; Wang, S.; Zhang, T.; Du, X.; Zhang, Y., Facet-charge-induced coupling dependent interfacial photocharge separation: a case of BiOI/g-C3N4 pn junction. *Applied Catalysis B: Environmental* **2020,** *267*, 118697.

14. Martin, D. J.; Reardon, P. J. T.; Moniz, S. J.; Tang, J., Visible light-driven pure water splitting by a nature-inspired organic semiconductor-based system. *Journal of the American Chemical Society* **2014,** *136* (36), 12568-12571.

15. Zhu, K.; Zhu, G.; Wang, J.; Zhu, J.; Sun, G.; Zhang, Y.; Li, P.; Zhu, Y.; Luo, W.; Zou, Z., Direct storage of holes in ultrathin Ni (OH) 2 on Fe 2 O 3 photoelectrodes for integrated solar charging battery-type supercapacitors.

Journal of Materials Chemistry A **2018,** *6* (43), 21360-21367.
16. Wang, P.; Chen, X.; Sun, G.; Wang, C.; Luo, J.; Yang, L.; Lv, J.; Yao, Y.; Luo, W.; Zou, Z., A capacitor‐type Faradaic junction for direct solar energy conversion and storage. *Angewandte Chemie International Edition* **2021,** *60* (3), 1390-1395.
17. Wang, Y.; Tang, J.; Peng, Z.; Wang, Y.; Jia, D.; Kong, B.; Elzatahry, A. A.; Zhao, D.; Zheng, G., Fully solar-powered photoelectrochemical conversion for simultaneous energy storage and chemical sensing. *Nano letters* **2014,** *14* (6), 3668-3673.
18. Xia, X.; Luo, J.; Zeng, Z.; Guan, C.; Zhang, Y.; Tu, J.; Zhang, H.; Fan, H. J., Integrated photoelectrochemical energy storage: solar hydrogen generation and supercapacitor. *Scientific reports* **2012,** *2* (1), 1-6.
19. Zhang, J.; Jiang, D.; Wang, P.; Zhong, J.; Sun, G.; Yao, Y.; Luo, W.; Zou, Z., A high-voltage solar rechargeable device based on a CoPi/BiVO 4 faradaic junction. *Journal of Materials Chemistry A* **2022,** *10* (4), 1802-1807.
20. Chen, X.; Zhu, K.; Wang, P.; Sun, G.; Yao, Y.; Luo, W.; Zou, Z., Reversible charge transfer and adjustable potential window in semiconductor/Faradaic layer/liquid junctions. *Iscience* **2020,** *23* (3), 100949.
21. Safshekan, S.; Herraiz-Cardona, I.; Cardenas-Morcoso, D.; Ojani, R.; Haro, M.; Gimenez, S., Solar Energy Storage by a Heterostructured BiVO4–PbO x Photocapacitive Device. *ACS Energy Letters* **2017,** *2* (2), 469-475.
22. Wang, P.; Xue, M.; Jiang, D.; Yang, Y.; Zhang, J.; Dong, H.; Sun, G.; Yao, Y.; Luo, W.; Zou, Z., Photovoltage memory effect in a portable Faradaic junction solar rechargeable device. *Nature communications* **2022,** *13* (1), 1-8.
23. Wang, Y.; Yao, E. P.; Wu, L.; Feldmann, J.; Stolarczyk, J. K., A Multi‐Layer Device for Light‐Triggered Hydrogen Production from Alkaline Methanol. *Angewandte Chemie* **2021,** *133* (51), 26898-26905.
24. Zhang, H.; Yang, L.; Zhang, P.; Lu, C.; Sha, D.; Yan, B.; He, W.; Zhou, M.; Zhang, W.; Pan, L., MXene‐Derived TinO2n− 1 Quantum Dots Distributed on Porous Carbon Nanosheets for Stable and Long‐Life Li–S Batteries: Enhanced Polysulfide Mediation via Defect Engineering. *Advanced Materials* **2021,** *33* (21), 2008447.
25. Han, Q.; Wu, C.; Jiao, H.; Xu, R.; Wang, Y.; Xie, J.; Guo, Q.; Tang, J., Rational design of high‐concentration Ti3+ in porous carbon‐doped TiO2 nanosheets for efficient photocatalytic ammonia synthesis. *Advanced Materials* **2021,** *33* (9), 2008180.
26. Yu, H.; Shi, R.; Zhao, Y.; Bian, T.; Zhao, Y.; Zhou, C.; Waterhouse, G. I.; Wu, L. Z.; Tung, C. H.; Zhang, T., Alkali‐assisted synthesis of nitrogen deficient graphitic carbon nitride with tunable band structures for efficient visible‐light‐driven hydrogen evolution. *Advanced Materials* **2017,** *29* (16), 1605148.
27. Seo, T.; Kurokawa, R.; Sato, B., A convenient method for determining the concentration of hydrogen in water: use of methylene blue with colloidal platinum. *Medical gas research* **2012,** *2* (1), 1-6.
28. Zhang, J.; Jin, Z.; Feng, C.; Yu, L.; Zhang, J.; Zhang, Z., ESR study on the visible photocatalytic mechanism of nitrogen-doped novel TiO2: Synergistic effect of two kinds of oxygen vacancies. *Journal of Solid State Chemistry* **2011,** *184* (11), 3066-3073.
29. Xiong, L.-B.; Li, J.-L.; Yang, B.; Yu, Y., Ti??+ in the Surface of Titanium Dioxide: Generation, Properties and Photocatalytic Application. *Journal of Nanomaterials* **2012,** *2012*.
30. Yu, X.; Kim, B.; Kim, Y. K., Highly enhanced photoactivity of anatase TiO2 nanocrystals by controlled hydrogenation-induced surface defects. *ACS Catalysis* **2013,** *3* (11), 2479-2486.
31. Kuznetsov, A.; Kameneva, O.; Alexandrov, A.; Bityurin, N.; Marteau, P.; Chhor, K.; Sanchez, C.; Kanaev, A., Light-induced charge separation and storage in titanium oxide gels. *Physical Review E* **2005,** *71* (2), 021403.
32. Savateev, O., Photocharging of Semiconductor Materials: Database, Quantitative Data Analysis, and Application in Organic Synthesis. *Advanced Energy Materials* **2022,** *12* (21), 2200352.
33. Chen, R.; Fan, F.; Dittrich, T.; Li, C., Imaging photogenerated charge carriers on surfaces and interfaces of photocatalysts with surface photovoltage microscopy. *Chemical Society Reviews* **2018,** *47* (22), 8238-8262.
34. Hankin, A.; Bedoya-Lora, F. E.; Alexander, J. C.; Regoutz, A.; Kelsall, G. H., Flat band potential determination: avoiding the pitfalls. *Journal of Materials Chemistry A* **2019,** *7* (45), 26162-26176.
35. Thangamuthu, M.; Ruan, Q.; Ohemeng, P. O.; Luo, B.; Jing, D.; Godin, R.; Tang, J., Polymer Photoelectrodes for Solar Fuel Production: Progress and Challenges. *Chemical Reviews* **2022**.
36. Hong, S. J.; Lee, S.; Jang, J. S.; Lee, J. S., Heterojunction BiVO 4/WO 3 electrodes for enhanced photoactivity of water oxidation. *Energy & Environmental Science* **2011,** *4* (5), 1781-1787.
37. Zhao, Y.; Shi, T.; Shang, J.; Ding, L.; Cao, X.; Chen, C.; Zhao, J., Rapid proton exchange between surface bridging hydroxyls and adsorbed molecules on TiO2. *Applied Catalysis B: Environmental* **2020,** *277*, 119234.
38. Prabhuram, J.; Manoharan, R., Investigation of methanol oxidation on unsupported platinum electrodes in strong alkali and strong acid. *Journal of Power Sources* **1998,** *74* (1), 54-61.
39. Yu, E. H.; Scott, K.; Reeve, R. W., A study of the anodic oxidation of methanol on Pt in alkaline solutions. *Journal of Electroanalytical Chemistry* **2003,** *547* (1), 17-24.
40. Hykaway, N.; Sears, W.; Morisaki, H.; Morrison, S. R., Current-doubling reactions on titanium dioxide photoanodes. *The Journal of Physical Chemistry* **1986,** *90* (25), 6663-6667.
41. Ahmed, A. Y.; Kandiel, T. A.; Ivanova, I.; Bahnemann, D., Photocatalytic and photoelectrochemical oxidation mechanisms of methanol on TiO2 in aqueous solution. *Applied surface science* **2014,** *319*, 44-49.
42. Kalamaras, E.; Lianos, P., Current Doubling effect revisited: Current multiplication in a PhotoFuelCell. *Journal of Electroanalytical Chemistry* **2015,** *751*, 37-42.
43. Gong, Y.; Tian, W.; Zhang, P.; Chen, J.; Zhang, Y.; Sun, Z., Slip casting and pressureless sintering of Ti3AlC2. *Journal of Advanced Ceramics* **2019,** *8* (3), 367-376.
44. Zheng, W.; Zhang, P.; Chen, J.; Tian, W.; Zhang, Y.; Sun, Z., In situ synthesis of CNTs@ Ti 3 C 2 hybrid structures by microwave irradiation for high-performance anodes in

lithium ion batteries. *Journal of Materials Chemistry A* **2018,** *6* (8), 3543-3551.